Volume 140 | Number 3 | 7 February 2015 | Pages 673–946

# Analyst

www.rsc.org/analyst

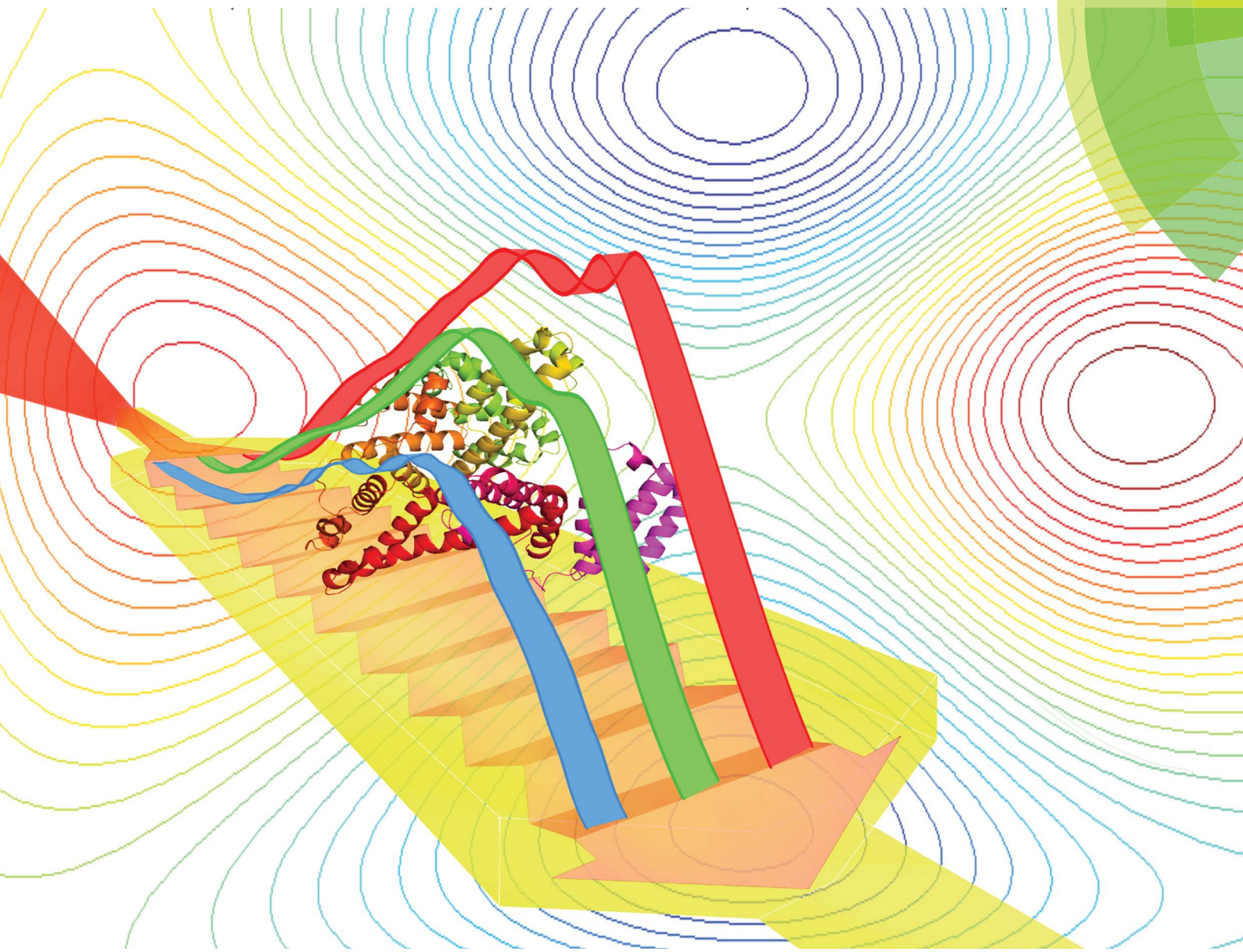

ISSN 0003-2654

ROYAL SOCIETY OF CHEMISTRY

PAPER
Han-Qing Yu, Boris Mizaikoff *et al.*
Probing the secondary structure of bovine serum albumin during heat-induced denaturation using mid-infrared fiberoptic sensors

Analyst

PAPER

View Article Online
View Journal | View Issue



Cite this: *Analyst*, 2015, **140**, 765

# Probing the secondary structure of bovine serum albumin during heat-induced denaturation using mid-infrared fiberoptic sensors

Rui Lu,[a] Wen-Wei Li,[a] Abraham Katzir,[c] Yosef Raichlin,[d] Han-Qing Yu*[a] and Boris Mizaikoff*[b]

Attenuated total reflection Fourier transform infrared (ATR-FTIR) spectroscopy using a special waveguide based on a silver halide fiber was used for probing the heat-induced secondary structure and conformation changes of bovine serum albumin (BSA). From the secondary derivative and the curve fitting of the obtained ATR-FTIR spectra, the changes of the BSA secondary structure with temperature were clearly identified. Two different thermal denaturation temperature ranges (*i.e.*, 50–52 and 80–82 °C, at which a change of the protein structure occurred) were determined, while only one denaturation temperature was previously identified *via* classical FTIR measurements. Additionally, taking advantage of two-dimensional correlation spectroscopy more detailed information on changes of the protein secondary structure was revealed. The developed method facilitates *in situ*, sensitive, and more in-depth probing of protein secondary structures, which represents a significant advancement compared to conventional characterization methods.

Received 14th August 2014
Accepted 11th November 2014

DOI: 10.1039/c4an01495b

www.rsc.org/analyst



## Introduction

Serum albumin is a versatile carrier protein, and one of the most important blood proteins. Especially, bovine serum albumin (BSA), which comprises a single-chain midsize protein composed of 583 amino acids with a molecular weight of approximately 66.5 kDa, has been extensively studied. The properties of BSA are strongly dependent on its secondary structure, which contains 67% helical structures next to 10% turn, and 23% extended chain configurations without any β sheets.[1] The BSA secondary structure can be affected by a range of physical and chemical factors including temperature, pressure, pH, and the presence of surfactants.[2–4] For instance, high temperature is known to cause protein denaturation by changing the protein secondary structure.

Such a heat-induced protein denaturation is detectable by various spectroscopic methods, including ultraviolet-visible (UV/Vis) spectroscopy, nuclear magnetic resonance (NMR) spectroscopy, circular dichroism (CD) methods in various wavelength regimes, fluorescence spectroscopy, Raman and Fourier transform infrared (FTIR) spectroscopy, and after crystallization *via* X-ray crystallography.[5,6] Among these techniques, FTIR has gained increasing relevance, because the vibrational spectrum is selective in the absorption band frequency position, widths, and intensities in response to protein structural changes.[7] The most distinct and characteristic FTIR bands of proteins are the amide signatures. In particular, the amide I band (1700–1600 $cm^{-1}$), which convolutes the major structural domain elements of proteins including α helix, β sheet, β turn, random coil, and anti-parallel intermolecular β sheet,[8] has frequently been used to reveal the secondary structure of a protein. For FTIR detection, only a small amount of protein sample (approximately 10–100 μg) is needed. Therefore, it offers a facile method to study heat-induced dynamics and associated secondary structure changes of BSA[6,7] and other proteins in aqueous solution.[2–4,9] However, conventional FTIR spectroscopy provides only limited detection accuracy and sensitivity for monitoring the protein denaturation processes. Among the most substantial challenges in this respect is the fact that the bands of individual domain elements constituting the secondary structure typically overlap with each other. As a consequence, a precise band assignment in the amide I region and a quantitative identification of the secondary structure become difficult. Therefore, to extract more useful and accurate information on the denaturation process, band deconvolution and assignment of FTIR spectra require further optimization.

A recent trend in this direction is applying attenuated total reflection (ATR) infrared spectroscopy, which enables the direct detection of analytes at solid/liquid interfaces. Silver halide fibers are increasingly adopted as a suitable waveguide material in ATR spectroscopy due to their broad infrared-transparent

[a]*Department of Chemistry, University of Science and Technology of China, Hefei 230026, P.R. China. E-mail: hqyu@ustc.edu.cn*
[b]*Institute of Analytical and Bioanalytical Chemistry, University of Ulm, 89081 Ulm, Germany. E-mail: boris.mizaikoff@uni-ulm.de*
[c]*School of Physics, Tel-Aviv University, Tel-Aviv 69978, Israel*
[d]*Department of Applied Physics, Ariel University Center of Samaria, Ariel, Israel*

window and a finely tunable flexible geometry.[10] Previously, planar-tapered silver halide fibers have been used to effectively detect specific molecular constituents,[11–13] to simultaneously determine multiple volatile organics,[14] or to analyze biomolecules.[15] The usage of fiberoptic waveguides as active sensing elements facilitates an increased number of internal inflections such that the intensity of the evanescent field and the resulting analytical signal can be significantly enhanced. However, to date there has been no report demonstrating the utility of such miniaturized fiberoptic sensors for probing protein structures or for advancing 2D correlation spectroscopy.

Here, a planar-tapered silver halide fiber was utilized for the first time to characterize protein denaturation processes. The heat-induced denaturation process of BSA was successfully identified by ATR-FTIR spectroscopy along with optimized band assignments. For the band assignments, we have employed a curve fitting method to extract detailed relevant information of structural variations from the temperature-dependent spectra. For the band sequential order,[16] we have introduced two-dimensional correlation spectroscopy (2DCoS)[17–19] to explore the secondary structural changes of BSA in detail.

# Experimental

### Chemicals

Crystallized powder of albumin from bovine serum (Lot 129H0913) was purchased from Sigma Inc. and was used without further treatment. Before the experiments, the protein was dissolved in $D_2O$ to a final defatted BSA concentration of 2.5%, and then stored at 4 °C for two days. In this study, $D_2O$ instead of $H_2O$ was used as a solvent to facilitate the characterization of proteins *via* FTIR spectroscopy, as $D_2O$ significantly reduces the strongly absorbing background of $H_2O$ within the spectral regime of interest,[20–23] while the peak location and characteristics of the protein spectra are preserved.

### Instrumentation

The FTIR spectra were recorded on a Bruker Vertor 22 spectrometer equipped with a liquid nitrogen cooled mercury cadmium telluride (MCT) detector. BSA was added into a homemade FTIR cell equipped with a planar silver halide fiber sensor. This sensor was fabricated providing a unique geometry, as previously described,[14] thereby yielding a planar segment with 290 μm thickness in the middle section tapering into 700 μm diameter cylindrical fiber segments at both ends. This geometry enables a particularly high number of internal reflections while maintaining efficient optical coupling. At each temperature, the spectral data within the band range of 4000 to 400 $cm^{-1}$ were recorded, and 64 scans were averaged for each spectrum with a spectral resolution of 2 $cm^{-1}$. The sample temperature was controlled using a feedback heating system. To obtain spectra at serial temperatures, the protein solutions were heated serially from 30 to 90 °C with an increment of 2 °C. The spectrum at each temperature was measured after equilibrating the sample for at least 5 min.

### Data processing

The OPUS 5.5 software (Bruker Co., Germany) was used for data processing. All original protein spectra were confined to the relevant spectral regime and baseline corrected between 1700 and 1600 $cm^{-1}$ for further analysis. Then, spectra were fitted with Gaussian band profiles by using PeakFit software (SeaSolve Software Inc., USA). The number of bands and positions were taken from their second derivative spectra. In the fitting process, the heights, widths, and positions of all bands were varied simultaneously.

### Two-dimensional correlation spectroscopy

Generalized 2DCoS has been used for analysis of various spectroscopic data by improving the spectra resolution and detecting the sequential order of events by 'sequential order' rules.[3,4,16–19] It allows cross-correlation analysis of the spectral series in response to some modulation variable (temperature in our case), and can create two-dimensional correlation maps with the same wavelength or wavenumber axis in both dimensions.[24] The 2D wavenumber–wavenumber correlation analysis provides two different correlation maps. The synchronous map shows correlations between all spectral bands changing in the experiment, that is, whether they increase or decrease relative to each other. The asynchronous correlation map relates the wavenumber that changes at different rates, and it also contains information about the sequence of event occurrence.[25] 2DCoS has been previously used as a powerful tool to study the changes of the amide I band,[9,26] and hence was employed here for the BSA denaturation study. All the calculations were performed using Matlab R2012a (Mathworks Inc., USA).

# Results and discussion

### ATR-FTIR and secondary derivative spectra

Fig. 1A shows the FTIR spectra of BSA after smoothing and baseline correction in the amide I region (1700–1600 $cm^{-1}$), which varied substantially with temperature. The band assignments in the amide I band region were determined referring to an earlier study.[7] In Fig. 1B, all the spectra are after two derivation treatments of original spectra in Fig. 1A. Such a two derivation treatment and the relatively high resolution of 2 $cm^{-1}$ might be two reasons for the occurrence of weak bands at 48 and 50 °C in Fig. 1B. From the second derivative spectra, a temperature-dependent variation in peak intensity can be more clearly observed for several characteristic bands.

For both the FTIR spectra and the second derivative spectra, the most distinct changes were determined in two dedicated temperatures ranges, *i.e.*, 50–52 °C and 80–82 °C. Specifically, when raising the temperature from 50 to 52 °C, the peak at 1662 $cm^{-1}$ disappeared, while a new peak at 1680 $cm^{-1}$ emerged. According to a previous study,[7] these two peaks should be ascribed to the β-turn. Subsequently, when the temperature was increased from 80 to 82 °C, the 1662 $cm^{-1}$ peak appeared again. Evidently, a substantial change of the protein structure

 

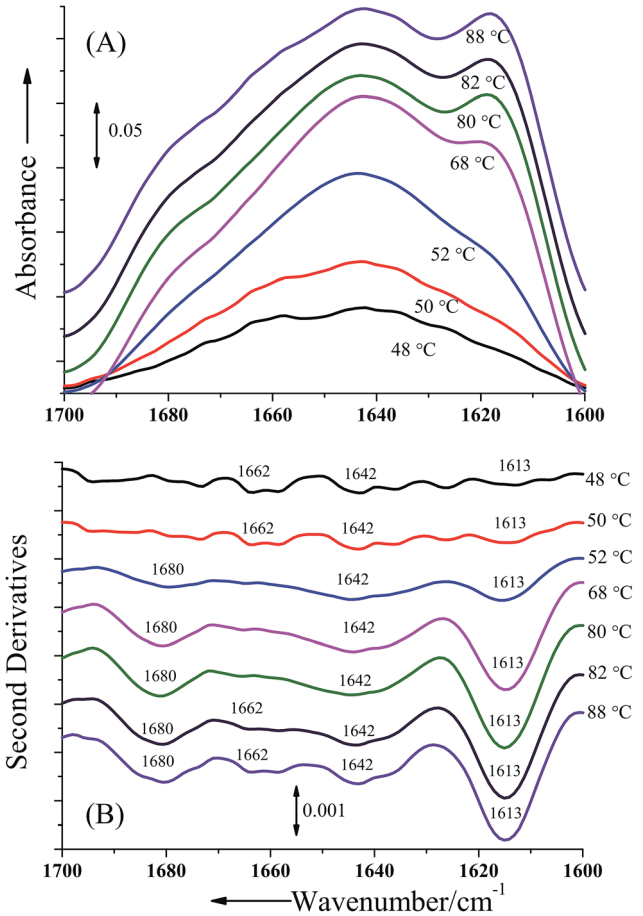


Fig. 1 ATR-FTIR spectra (A) and second derivative spectra (B) of BSA in $D_2O$ as a function of temperature at 48, 50, 52, 68, 80, 82, and 88 °C, respectively (after smoothing and baseline correction).

must have occurred in these distinct temperature ranges. Another noticeable peak is at 1613 $cm^{-1}$, whose intensity increased markedly with increasing temperature. Since this peak is mainly associated with the intermolecular β-sheet structure resulting from the aggregation,[7] our results strongly imply an irreversible aggregation of the protein and formation of the β-sheet structures. Combining these results, it can be derived that protein aggregation occurred at 50–52 °C, during which the unfolding of BSA became irreversible after the formation of intermolecular β-sheets.

It should be noted here that two different thermal denaturation temperature ranges were directly and distinctly observed in our study, which is attributed to the application of the planar-tapered silver halide fibers during the ATR-FTIR analysis. Given the significantly enhanced signal-to-noise ratio in contrast to using conventional, *i.e.*, macroscopic multi-reflection ATR crystals, these distinct denaturation ranges have been IR-spectroscopically visualized in such a pronounced fashion for the first time. Consequently, the developed measurement technique along with the obtained results present a substantial improvement compared to the conventional FTIR measurements, as further detailed below.

### Curve fitting for ATR-FTIR spectra

Based on our results and referring to related research,[7] the temperature-dependent protein denaturation process could be divided into three main temperature ranges: low temperature (<52 °C), medium temperature (52–80 °C), and high temperature (>82 °C). Therefore, to better characterize the BSA structure at each stage, three representative temperatures at different stages (*i.e.*, 48, 68, and 88 °C) were selected for further studies. To understand the contribution of each spectral (*i.e.*, band) component to the entire amide I contour, curve fitting of the ATR-FTIR spectra of BSA at each selected temperature was conducted (Fig. 2).

The fitting curves of the BSA spectra at 48 °C reveal 6 relevant bands (1613, 1632, 1642, 1662, 1670, and 1690 $cm^{-1}$) (Fig. 2A). Here, the bands at 1613 $cm^{-1}$ are assigned to heating-induced intermolecular β-sheet structures, while 1642 $cm^{-1}$ reflects random coils, 1662, 1670 and 1690 $cm^{-1}$ are attributed to β-turns.[6,7] However, the assigning of the band at near 1632 $cm^{-1}$

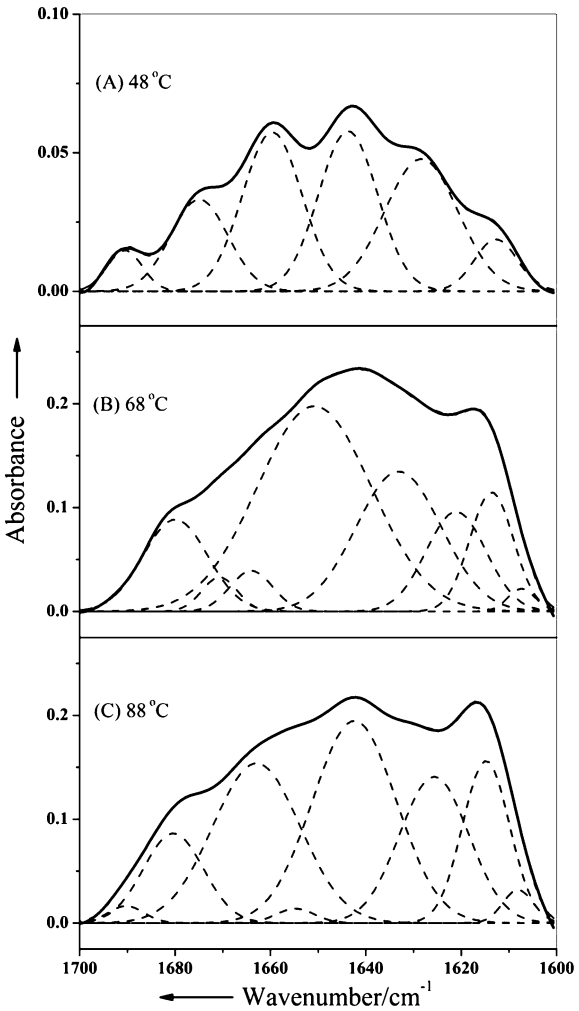


Fig. 2 Deconvoluted ATR-FTIR spectra of the BSA solution in the amide I region together with the respective best-fitted individual band components at 48 °C (A), 68 °C (B), and 88 °C (C). Solid and dotted lines indicate the experimental data and the individual Gaussian components, respectively.

Table 1 Frequencies ($cm^{-1}$) and assignments of IR bands of albumin in $D_2O$ solution (according to second derivatives)

| Wavenumber/$cm^{-1}$ | Assignment |
|---|---|
| 1680–1690 | β-turn |
| 1662–1670 | β-turn |
| 1650–1655 | α-helix |
| 1642–1645 | Random coil |
| 1632–1638 | Short-segment chains connecting the α-helical segment |
| 1610–1620 | Intermolecular β-sheet |

has been under controversy. Although it has been assigned to an intra-molecular β-sheet structure for many proteins,[27] several other studies suggest that it could be associated with the short segment chains connecting α-helix segments for some other proteins.[28,29] A later study convinces that for BSA this band is not ascribed to the intra-molecular β-sheet structure.[7] Therefore, here we assign the peak at 1630 $cm^{-1}$ to the short segment chains connecting α-helix segments. This interpretation also suggests that the secondary structures of BSA are more flexible and strongly exposed to the solvent.

The bands obtained after fitting the spectrum at 68 °C were located at 1608, 1613, 1620, 1632, 1650, 1662, 1670, and 1680 $cm^{-1}$ (Fig. 2B). Compared with those at lower temperatures, two of the bands (1642 and 1690 $cm^{-1}$) disappeared, while four new bands (1608, 1620, 1650, 1680 $cm^{-1}$) were observed. These new bands are assigned to the vibration of some amino acid residues, intermolecular β-sheet structure, α-helix, and β-turn, respectively.[6,7]

When further elevating the temperature to 88 °C, also eight bands were obtained after deconvolution (Fig. 2C). It is interesting to note that the two disappeared bands (1642 and 1690 $cm^{-1}$) emerged again. Five of the bands observed at 68 °C (1608, 1613, 1620, 1662, 1680 $cm^{-1}$) remained, and one new band occurred at 1655 $cm^{-1}$. This band is assigned to the α-helix content, possibly resulting from a shift of the 1650 $cm^{-1}$ band in the medium temperature range. All determined FTIR band assignments are summarized in Table 1. Apparently, fitting the FTIR spectral data within the amide I region using Gaussian band profiles facilitated the detailed identification of an increased number of individual band components, and therefore the efficient extraction of significantly more relevant information on BSA secondary structure changes compared to previously reported conventional methods.[7]

## IR absorbance of each band

Fig. 3 shows the temperature-dependent variations in peak intensity (estimated by peak area integral) of each band within the amide I region. After the temperature reached 54 °C, the peak intensity of the 1650 $cm^{-1}$ band increased markedly, due to the formation of a random coil of BSA. Meanwhile, the 1642 $cm^{-1}$ band that represents the random coil disappeared. The intensities of other bands were all substantially altered at this temperature. Likewise, significant changes in band intensities also occurred once the temperature was further elevated

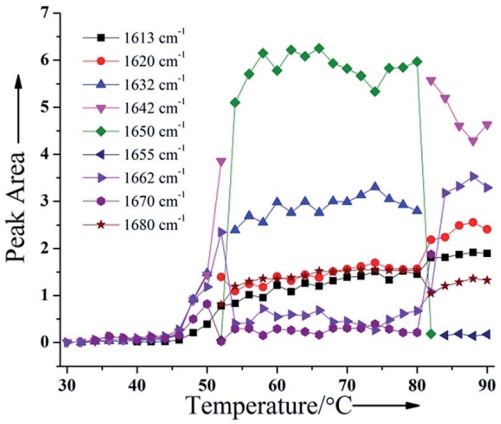


Fig. 3 IR absorbance (*i.e.*, peak area) represented as a function of temperature at the fitted wavenumbers.

to >80 °C. Thus, further convincing evidence is provided that the BSA conformation has been subject to two distinct regimes of changes at 50–52 °C and 80–82 °C, respectively during the heat-induced denaturation process.

## Two-dimensional ATR-FTIR correlation spectra

Fig. 4 illustrates the corresponding 2DCoS for the ATR-FTIR spectra of BSA obtained during the heat-induced denaturation process. The band positions derived from the two-dimensional

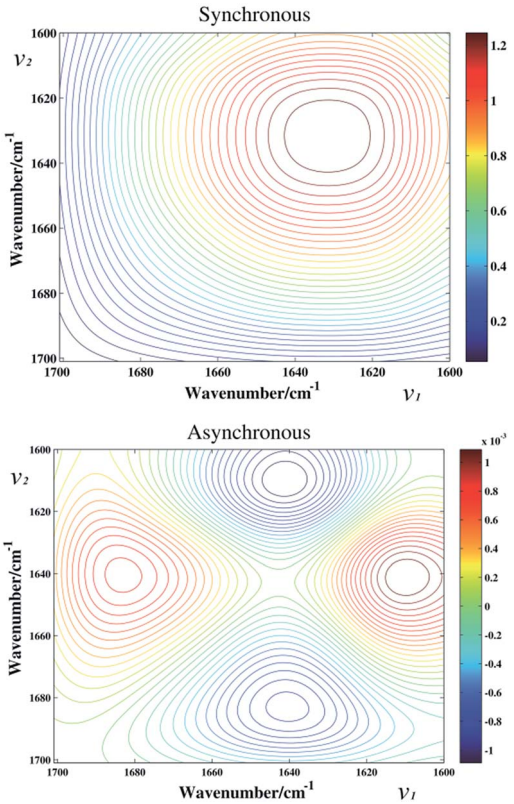


Fig. 4 Synchronous and asynchronous 2D ATR-FTIR correlation spectra constructed from 31 spectra recorded at 2 °C BSA during thermal transition from 30 to 90 °C.

Table 2 Signs of synchronous ($\Phi$) and asynchronous ($\Psi$) cross peaks and sequential order

| ($\nu_1$, $\nu_2$) | $\Phi$ ($\nu_1$, $\nu_2$) | $\Psi$ ($\nu_1$, $\nu_2$) | Sequential order |
|---|---|---|---|
| (1610, 1642) | + | + | 1610 > 1642 |
| (1642, 1686) | + | − | 1642 < 1686 |

correlation plots are summarized in Table 2. According to Noda rules, the 'sequential order' derives as follows: the sign of an asynchronous cross-peak becomes positive if the intensity change at $\nu_1$ occurs predominately before $\nu_2$. On the other hand, the peak sign becomes negative if the change at $\nu_1$ occurs predominately after $\nu_2$. However, such sign rules are reversed if the synchronous correlation intensity at the same coordinate becomes negative. $\nu_1$ and $\nu_2$ represent two independent spectral variables along the external variable temperature, and therefore the 'sequential order' provides useful information on the observed changes along the external variable.

From the signs of the synchronous cross-peaks at (1610, 1642) and (1642, 1686) (listed in Table 2), the 'sequential order' of the intensity changes of the three bands during the heating process was obtained as: 1610 > 1642 $cm^{-1}$, 1642 < 1686 $cm^{-1}$. Since the three bands represent intermolecular β-sheet (1610 $cm^{-1}$), random coil (1642 $cm^{-1}$), and β-turn (1686 $cm^{-1}$), respectively, the band sequential orders obtained here thus imply that both the intermolecular β-sheet and β-turn are more sensitive than the random coil to temperature. Thus, they underwent the most significant changes at increasing temperature.

Thus, sensitive and detailed probing of the heat-induced denaturation process of BSA was achieved in our study, attributed to the use of ATR-FTIR spectroscopy based on planar-tapered silver halide waveguide elements along with optimized band assignments and the band sequential order. The use of spectral curve fitting and 2DCoS analysis offered additional detailed information on the secondary structural change orders and thermal dynamics of BSA, thereby greatly advancing the detection of BSA structural changes.

Compared with conventional FTIR measurements, the developed ATR-FTIR probe with planar silver halide fibers as waveguides not only enables *in situ* measurements, but also significantly reduces the background absorbance while increasing the targeted analytical signal. Thereby, significantly more sensitive and reliable probing of protein structures under complex environmental conditions is achieved. Several remarkable improvements of our methodology in comparison with previous researches are noticeable. Firstly, the analysis of the secondary derivative ATR-FTIR spectra within the characteristic amide I (1600–1700 $cm^{-1}$) regime at different temperatures clearly revealed two distinct thermal denaturation ranges for BSA, at which a change of the protein structure occurred (Fig. 1B, 2 and 3). To date, however, only one temperature has been identified from the secondary derivative spectra obtained *via* conventional FTIR measurements within the same spectral range (1700–1600 $cm^{-1}$),[7] while for the first denaturation temperature an additional spectral regime was further needed. Secondly, with the relatively high resolution of spectra scanning, more individual components bands can be revealed compared to conventional FTIR measurements (Fig. 2). Lastly, ATR-FTIR exhibited significantly higher intensities of the individual components convoluted into the spectrum (Fig. 3). Thus, the developed methodology apparently reveals more detailed information on the protein structure changes compared to conventional techniques.

## Conclusions

In summary, our work provides an innovative analytical strategy to greatly improve the accuracy and sensitivity of FTIR spectroscopy for the detection of protein secondary structure changes in comparison to conventional FTIR methods, and may therefore promote the practical application of FTIR detection technologies in biodiagnostics. In future studies, next generation planar semiconductor waveguides will be implemented,[30–33] which provide a yet unprecedented level of miniaturization along with a substantial sensitivity increase, which may pave the way toward hand-held bioassays based on label-free mid-infrared sensing technologies. Notably, while the present study focuses on advanced insight related to temperature-dependent structural changes of BSA, probing conformational changes and aggregation properties of proteins such as α-synuclein, which is associated with neurodegenerative diseases such as *e.g.*, Parkinson's, warrants highly relevant investigations using the developed methodologies in future.

## Acknowledgements

The authors wish to thank the Program for Changjiang Scholars and Innovative Research Team in University, China for the partial support of this work.

## Notes and references

1 R. G. Reed, R. C. Feldhoff, O. L. Clute and T. Peters, *Biochemistry*, 1975, **14**, 4578–4583.
2 D. Charbonneau, M. Beauregard and H.-A. J. Tajmir-Riahi, *J. Phys. Chem. B*, 2009, **113**, 1777–1784.
3 K. Murayama, Y. Wu, B. Czarnik-Matusewicz and Y. Ozaki, *J. Phys. Chem. B*, 2001, **105**, 4763–4769.
4 Y. Wu, K. Murayama, B. Czarnik-Matusewicz and Y. Ozaki, *Appl. Spectrosc.*, 2002, **56**, 1186–1193.
5 B. Yuan, K. Murayama, Y. Wu, R. Tsenkova, X. Dou, S. Era and Y. Ozaki, *Appl. Spectrosc.*, 2003, **57**, 1223–1229.
6 B. Yuan, K. Murayama and H. Yan, *Appl. Spectrosc.*, 2007, **61**, 921–927.
7 K. Murayama and M. Tomida, *Biochemistry*, 2004, **43**, 11526–11532.
8 J. Zhang and Y. Yan, *Anal. Biochem.*, 2005, **340**, 89–98.
9 H. Huang, J. Xie and H. Chen, *Analyst*, 2011, **136**, 1747–1752.
10 B. Mizaikoff, *Anal. Chem.*, 2003, **75**, 258A–267A.
11 T. Schädle, A. Eifert, C. Kranz, Y. Raichlin, A. Katzir and B. Mizaikoff, *Appl. Spectrosc.*, 2013, **67**, 1057–1063.

12 C. Charlton, A. Katzir and B. Mizaikoff, *Anal. Chem.*, 2005, **77**, 4398–4403.
13 B. Mizaikoff, *Chem. Soc. Rev.*, 2013, **42**, 8683–8699.
14 R. Lu, G. Sheng, W. Li, H. Yu, Y. Raichlin, A. Katzir and B. Mizaikoff, *Angew. Chem., Int. Ed.*, 2013, **52**, 2265–2268.
15 U. Bindig, M. Meinke, I. Gersonde, O. Spector, I. Vasserman, A. Katzir and G. Muller, *Sens. Actuators, B*, 2001, **74**, 37–46.
16 I. Noda and Y. Ozaki, in *Two-Dimensional Correlation Spectroscopy – Applications in Vibrational and Optical Spectroscopy*, John Wiley & Sons, Ltd, 2005, pp. 217–230.
17 I. Noda, A. E. Dowrey, C. Marcoli, G. M. Story and Y. Ozaki, *Appl. Spectrosc.*, 2000, **54**, 236A–248A.
18 C. P. Schultz, O. Bârzu and H. H. Mantsch, *Appl. Spectrosc.*, 2000, **54**, 931–938.
19 Y. M. Jung, B. Czarnik-Matusewicz and Y. Ozaki, *J. Phys. Chem. B*, 2000, **104**, 7812–7817.
20 T. Lefèvre, M. Subirade and M. Pézolet, *Biomacromolecules*, 2005, **6**, 3209–3219.
21 L. L'Hocine, J. I. Boye and S. Jouve, *J. Agric. Food Chem.*, 2007, **55**, 5819–5826.
22 D. Neubauer, J. Korbmacher, M. Frick, J. Kiss, M. Timmler, P. Dietl, O. Wittekindt and B. Mizaikoff, *Anal. Chem.*, 2013, **85**, 4247–4250.
23 J. P. Korbmacher, C. Michel, D. Neubauer, K. Thompson, B. Mizaikoff, M. Frick, P. Dietl and O. H. Wittekindt, *Physiol. Rep.*, 2014, **2**, e00201.
24 I. Noda, *Appl. Spectrosc.*, 1993, **47**, 1329–1336.
25 A. Dominguez-Vidal, M. P. Saenz-Navajas, M. J. Ayora-Canada and B. Lendl, *Anal. Chem.*, 2006, **78**, 3257–3264.
26 M. Sanchez, F. J. Aranda, M. J. Espuny, A. Marques, J. A. Teruel, A. Manresa and A. Ortiz, *Langmuir*, 2008, **24**, 6487–6495.
27 D. Reinstädler, H. Fabian, J. Backmann and D. Naumann, *Biochemistry*, 1996, **35**, 15822–15830.
28 W. C. Reisdorf and S. Krimm, *Biochemistry*, 1996, **35**, 1383–1386.
29 R. Gilmanshin, S. Williams, R. H. Callender, W. H. Woodruff and R. B. Dyer, *Proc. Natl. Acad. Sci. U. S. A.*, 1997, **94**, 3709–3713.
30 X. Wang, J. Antoszewski, G. Putrino, W. Lei, L. Faraone and B. Mizaikoff, *Anal. Chem.*, 2013, **85**, 10648–10652.
31 M. Sieger, F. Balluff, X. Wang, S. S. Kim, L. Leidner, G. Gauglitz and B. Mizaikoff, *Anal. Chem.*, 2012, **85**, 3050–3052.
32 X. Wang, S. S. Kim, R. Rossbach, M. Jetter, P. Michler and B. Mizaikoff, *Analyst*, 2012, **137**, 2322–2327.
33 C. Charlton, M. Giovannini, J. Faist and B. Mizaikoff, *Anal. Chem.*, 2006, **78**, 4224–4227.